Fifth International Symposium on Marine Propulsors
smp'17, Espoo, Finland, June 2017

Comparison of Different Methods for Estimating Energetics Related to Efficiency on a UUV with Cephalopod Inspired Propulsion

Michael Krieg[1,3], **Kamran Mohseni**[1,2,3]

[1]Department of Mechanical and Aerospace Engineering,
[2]Department of Computer and Electrical Engineering,
[3]Institute for Networked Autonomous systems, University of Florida, Gainesville, Florida

ABSTRACT

In this paper we investigate an unmanned underwater vehicle which utilizes a set of novel cephalopod inspired pulsed jet thrusters. Recent studies on live squid suggest that the efficiency of this type of propulsor may be significantly higher than previously assumed Bartol et al. (2009). However, there is little experimental data of efficiency on underwater vehicles with this style of propulsion, due to their recent development. Furthermore, as the technology is fundamentally different from traditional propeller style thrusters, standard efficiency approximations are insufficient. This study is a first step towards experimental testing of the propulsive efficiency of this technology. We examine three different methods for estimating control forces, as will be necessary to calculate useful propulsive work. These include: modeling propulsive jet impulse, modeling pressure distribution within the thruster mechanism, and backing out control forces from hydrodynamic force estimates and vehicle inertial forces measured with a motion capture system. All three control force measurement techniques showed good agreement for a variety of maneuvers, validating the different assumptions of the individual models.

We also look into two methods for estimating the work done on the surrounding fluid environment required to create the propulsion. It was observed that estimating total required work from the excess kinetic energy in the wake will always under-predict the actual total work due to viscous dissipation of kinetic energy prior to measurement of the wake energy, and that a more accurate estimate can be achieved by integrating the product of pressure and boundary velocity on the surface of the thruster mechanism.

Keywords

Propulsive Output, Unrestrained UUVs, Control Forces, Energetics.

Corresponding Author: Mohseni@ufl.edu

1 INTRODUCTION

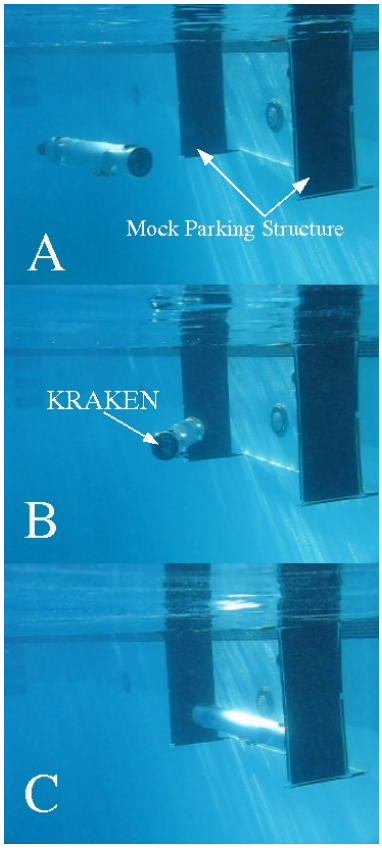

Figure 1: Successive frames of a UUV with squid inspired thrusters performing a mock parallel parking maneuver.

As the use of unmanned underwater vehicles (UUVs) increases in both autonomous missions and missions requiring human-robot interactions, there is an increased need for enhanced vehicle capabilities. One such desirable capability is improved position tracking accuracy in turbulent environments. Accurate low speed maneuvering in any environment, chaotic or not, is difficult for underwater vehicles to achieve without sacrificing efficient forward locomotion. Typically autonomous underwater vehicles that are designed for long range missions have a slender torpedo

shaped body to maximize efficiency of forward propulsion, and control surfaces generate maneuvering forces. When such a vehicle is traveling with little or no forward velocity, the forces from control surfaces become negligible, making turning (yaw) or sideways translation (sway) impossible. Vehicles designed for missions which require higher accuracy maneuvering; alternatively, have thrusters attached to several points around the surface of the vehicle providing full control over the six degrees of freedom, but inducing significant drag losses during long range transit.

Our group has proposed that long range torpedo shaped vehicles can achieve high accuracy low speed maneuvering utilizing cephalopod inspired jet thrusters that can be placed internal to the UUV hull surface Mohseni (2006), minimizing impact on forward drag while providing control forces in the absence of forward velocity. We have demonstrated the feasibility of such systems with multiple UUV prototypes Krieg et al. (2011). These thrusters, like squid and jellyfish, cyclically suck in some of the surrounding seawater then eject it as a high momentum propulsive jet. Even though there is zero net mass flux during an entire cycle, there is a positive flux of momentum and energy associated with the jetting. The thrusters offer several advantages. Aside from the negligible impact on forward drag already mentioned, the thrusters provide control forces instantaneously, unlike propeller based thrusters Yoerger et al. (1990) or tunnel thrusters Mclean (1991) for example.

However, jet propulsion has long been assumed to be inherently inefficient Lighthill (1969); Vogel (1994), as thrust scales with jet velocity squared and power scales with jet velocity cubed for steady jets. Recent studies, however, have reported propulsive efficiency as high as 78% in adult *L. brevis* swimming at high velocities, and averaged 87% (6.5%) for paralarvae Bartol et al. (2009), challenging the notion that a low volume high velocity jet inherently negates a high propulsive efficiency. The unexpectedly high efficiency of this mode of swimming is likely due, in large part, to the formation of a leading vortex ring associated with unsteady jetting, which is known to affect pressure dynamics at the nozzle exit Krueger (2005)Krieg & Mohseni (2013).

Due to the novelty of this type of propulsion there has been very little investigation into the efficiency dynamics associated with different types of maneuvers. The goal of the current study is to resolve several issues related to experimentally measuring the propulsive efficiency of this type of thruster on a freely moving UUV, specifically the most accurate ways of measuring control forces and total power transfer to the surrounding fluid without restricting the motion of the UUV.

2 VEHICLE DESCRIPTION

The UUV used for this experiment is the most recent of several vehicle platforms designed to showcase a new style of underwater propulsion. The vehicle, shown in figure 2, has a long slim torpedo shaped body with a propeller in the rear, and four internal pulsed jet thrusters to provide maneuvering forces. The vehicle is described in great detail in Krieg et al. (2011).

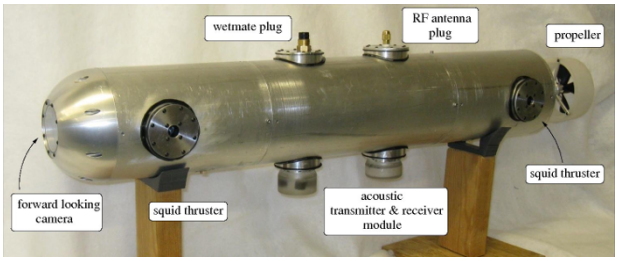

Figure 2: Picture of the newest generation UUV with squid inspired thrusters and other systems labeled. More detail of the vehicle can be found in Krieg et al. (2011).

2.1 Dimensions and Overall Performance

The UUV is 15 cm in diameter and 1.12 m in length with a total mass (including ballast) of 64.5kg. With thrusters operating at frequencies approaching cavitation frequency, which is a limiting frequency for proper thruster operation Krieg & Mohseni (2008), the vehicle has a maximum sway velocity of 0.12m/s (roughly equal to one body diameter per second). The vehicle has a maximum forward velocity of 0.56m/s (roughly 0.5 body lengths per second).

2.2 Cephalopod Inspired Thrusters

Much like squid, octopus, cuttlefish and other cephalopods, from which it draws inspiration, our thruster consists of an internal fluid cavity that can deform to change the internal volume. At the cavity interface with the vehicle hull there is a small circular orifice exposed to the outer water. The cavity of the thruster provides the same functionality as the squid mantle or the jellyfish bell, expanding and contracting to cycle water in and out of the circular orifice (functionally similar to the squid funnel/siphon). The cavity has a cylindrical shape with a flat circular plate at the back called the 'plunger'. The side wall is made of flexible rubber, but reinforced with helical supports so that it can deform in the axial direction allowing the plunger to move back and forth, but maintains a consistent diameter.

3 EXPERIMENTAL SETUP

3.1 Testing Tank

The prototype UUV described in section 2 is tested within a large cylindrical water tank. The tank, which is shown in figure 3, is 7.6 m in diameter and 4.9 m deep with a total volume of 2.46 kl. An aluminum platform runs across one edge of the tank, providing 5.5 m of access to the water surface.

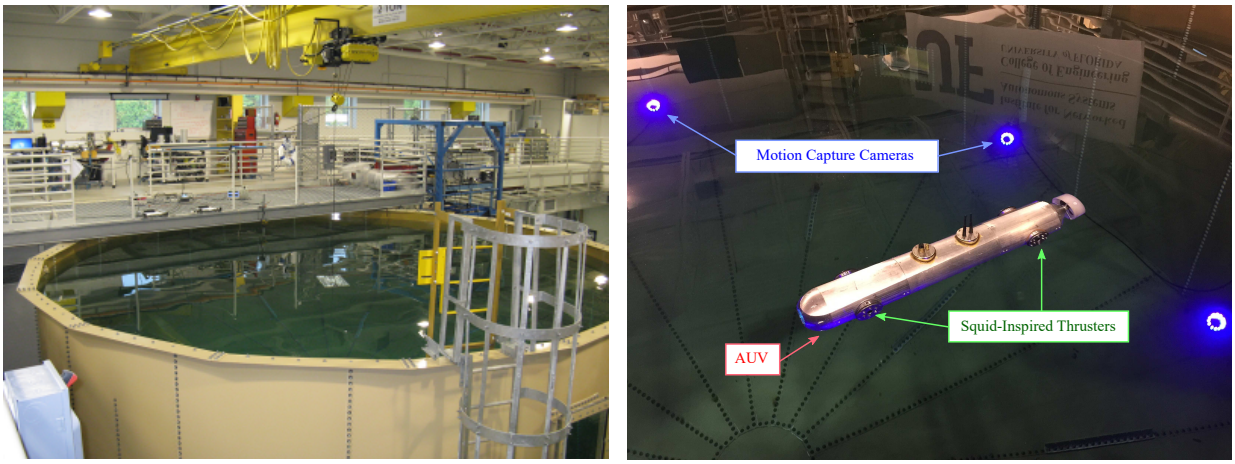

(UUV Testing Tank) (View Inside Tank)

Figure 3: Large water tank used to test UUV prototypes, showing the underwater motion capture system.

3.2 Motion Capture System

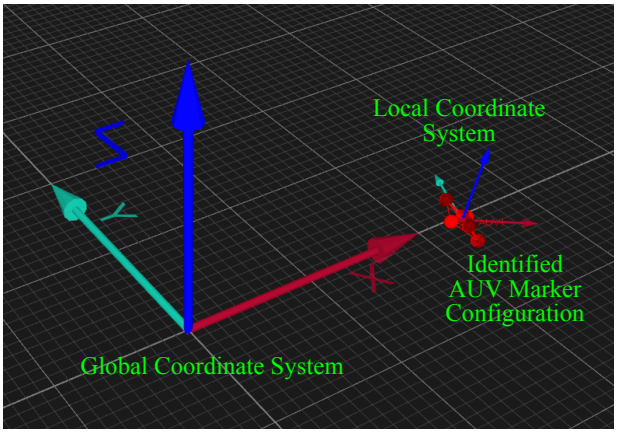

Figure 4: Screenshot of the virtual testing environment recorded by the motion capture system. It can be seen that the markers on the UUV are identified as a set configuration with an associated local coordinate system.

The exact trajectory and orientation of the UUV throughout different maneuvers are determined and recorded by an underwater motion capture system installed within the vehicle testing tank. The system consists of 6 Oqus 510+ underwater motion capture cameras, which can operate in both marker identification mode and video capture mode, with a maximum frame rate of 250 fps. Multiple cameras are shown installed within the tank in figure 3. Prior to each UUV testing session the motion capture system was calibrated with an average residual of 1.78 mm $\pm$0.25 mm. The residual during calibration can be considered the accuracy of the position measurement of the UUV. This average residual corresponds to an error of ± 0.025 rad in the measured orientation of the vehicle, which is determined from the position of markers on the vehicle surface relative to each other. The markers on the vehicle surface are made of retro-reflective tape, so that they do not project out from the vehicle surface or affect the vehicle drag properties.

3.3 Maneuver Descriptions

There are three basic types of maneuvers performed by the UUV in this study: sideways translation along the y-axis (sway), rotation about the z axis (yaw), and forward translation along the x-axis (surge).

4 UUV ENERGETICS ASSOCIATED WITH PROPULSIVE EFFICIENCY

In the most general sense the propulsive efficiency, η_{prop}, of an underwater vehicle is the ratio of the useful propulsive work, W_P, (sometimes referred to as the thrust work) to the total work required to generate the propulsion, W_T. Here, these characteristic quantities will be defined using nomenclature consistent with Fossen (1994).

$$W_P = \int_{t_0}^{t_f} \vec{F}_C \cdot \dot{\vec{\eta}}\, dt = \int_{t_0}^{t_f} \vec{\tau}_C \cdot \vec{\nu}\, dt \ , \tag{1}$$

$$\vec{\eta} = [X, Y, Z, \phi, \theta, \psi]^T \ , \tag{2}$$

$$\vec{\nu} = [u, v, w, p, q, r]^T \ , \tag{3}$$

where η is the position/orientation of the vehicle in an inertial frame, $[X, Y, Z]$ are positions in the inertial frame, $[\phi, \theta, \psi]$ are Euler angles; ν is a vector for the linear and angular velocities in the body fixed coordinate system, $[u, v, w]$ are the body fixed velocities in the surge, sway, and heave directions, and $[p, q, r]$ are the angular velocities about each respective body fixed axis; τ_C is a vector of the control forces/torques in the body fixed frame; F_C are the control forces and torques acting on the body in the direction of the inertial frame axes; and t_0 and t_f are the initial and final times, respectively, of the maneuver. Clearly the definition of the propulsive work in the body-fixed frame has the advantage that the propulsors on the UUV have a fixed layout in this coordinate frame.

The total work required to create the necessary propulsive forces (τ_C and F_C) is specific to the particular method of actuation, and hence not easily determined from vehicle

kinematics alone. In the following sections we will describe several different approaches for backing out the useful propulsive work and the total work needed to calculate propulsive efficiency.

4.1 Estimating Control Forces on a Freely Swimming Vehicle

Calculating the useful propulsive work, equation (1), requires that the 6 component UUV velocity and control force/torque vectors are known in either the inertial or body-fixed coordinates. The inertial velocity vector is measured directly by the motion capture system, and is easily converted between the two coordinate systems. However, measuring control forces acting on a freely moving vehicle is more difficult, since directly attaching the vehicle to some form of force balance would restrict its movement. Here we describe how the control forces can be recovered by various methods.

4.1.1 Calculating Jet Forces From Motor Frequency

The total hydrodynamic impulse, I, of each expelled jet is equivalent to the net impulse transferred to the UUV over the full pulsation cycle. Therefore, the average thrust produced is equal to the product of the hydrodynamic impulse of a single jet and the jet pulsation frequency. It should be noted; however, that the instantaneous thrust is not necessarily equal to the rate at which impulse is created in the jet since there are additional unsteady forces, as will be discussed in the next section, that have no net contribution to the average thrust over an entire cycle.

The rate at which hydrodynamic impulse is created in starting jets, including the contributions from vortex ring formation and nozzle geometry, was derived in Krieg & Mohseni (2013) as,

$$\frac{dI}{dt} = \rho\pi\left(g + \frac{k_2^\star - k_1^\star}{4}\right) u_b(t)^2 \frac{R_p^4}{R^2} \ . \tag{4}$$

Here, $u_b(t)$ is the velocity of the plunger inside the cavity, R_p is the radius of the plunger, R is the radius of the nozzle, $k_1^\star$ is the non-dimensional slope of the radial velocity profile at the nozzle exit, $k_2^\star$ is the non-dimensional slope of the radial velocity gradient, and g is a function related to the axial velocity profile at the nozzle. The terms $k_1^\star$, $k_2^\star$, and g are characterized for different nozzle geometries in Krieg & Mohseni (2013), but for the thrusters installed on the UUV the following values are a good approximation $k_1^\star = -0.5$, $k_2^\star = 1.1$, $g = 1.25$. Furthermore, the plunger driving mechanism on the UUV creates a sinusoidal jet velocity program, so that the average thrust, $\bar{T}$, can be calculated by integrating equation (4),

$$\bar{T}(f) = 2\rho\pi^3 R^4 \left(g + \frac{k_2^\star - k_1^\star}{4}\right)\left(\frac{L}{D}\right)^2 f^2 \ , \tag{5}$$

where f is the pulsation frequency and L/D is the stroke ratio of the jet. For the thrusters studied here $L/D = 3$.

4.1.2 Unsteady Internal Pressure Modeling

Even though the net impulse transfer during a single pulsation is equal to the hydrodynamic impulse of the propulsive jet, the instantaneous forces created during jetting include forces due to acceleration and deceleration of fluid inside the jetting cavity. These forces are cyclical, and thus make no net contribution to the impulse transfer over an entire cycle. However, work is required to create the internal fluid oscillations. Here we will describe a technique for analytically modeling the unsteady pressure distribution inside the thruster cavity, which can be used to calculate instantaneous thrust, and the total work is calculated in the following section.

It was recognized in Krieg & Mohseni (2015) that the central axis of axisymmetric jet flows is inherently irrotational, despite complicated vorticity patterns throughout the rest of the domain. This allows internal pressure to be related to stagnation pressure by integrating the momentum equation along the axis. In addition, the closed loop velocity integrals defining circulation in the cavity and jet regions can be segmented into velocity line integrals that show up in the integral of the momentum equation. We will not present the complete derivation of internal pressure; however, as defined in Krieg & Mohseni (2015), the relationship between internal pressure and system circulation is,

$$\frac{P_b}{\rho} = \frac{P_\infty}{\rho} + \frac{d\Gamma_{Jet}}{dt} + \frac{d\Gamma_{Cav}^\star}{dt} + \frac{1}{2}u_b^2 \ , \tag{6}$$

where P_∞ is stagnation pressure, P_b is the pressure on the internal surface of the cavity plunger, u_b is the velocity of the plunger, Γ_{Jet} is the circulation of the propulsive jet, $\Gamma_{Cav}^\star$ is the circulation inside the cavity neglecting the circulation created by boundary stretching.

With the exception of a few locations where vorticity is generated (i.e. at the nozzle edge and cavity surface) vorticity is just diffused without increasing or decreasing overall circulation. Therefore, the evolution of system circulation, $\frac{d\Gamma_{Jet}}{dt}$ and $\frac{d\Gamma_{Cav}}{dt}$, can be calculated by modeling the finite number of vorticity sources.

Unsteady cavity-jet systems have four distinct sources of vorticity that are identified and modeled in Krieg & Mohseni (2015). Though all the details of these models are too lengthy to discuss in this paper, here we will summarize each vorticity source and how they depend on thruster operating conditions. The first source is the flux of vorticity carried in the shear layer created at the nozzle edge by fluid either exiting or entering the cavity. The rate of vorticity flux is proportional to the square of the jet velocity squared. The second source of vorticity is associated with fluid converging before it passes through the nozzle. This vorticity can be modeled by the potential flow of a disc shaped velocity sink and increases system circulation proportional to the jet acceleration. The third vorticity generation mechanism only exists during the refill phase of the pulsation

cycle. It occurs when the leading vortex ring from incoming fluid impinges upon the inner cavity surface, which results in a boundary layer being formed on the surface of opposite sign vorticity. The fourth source is due to stretching of the cavity surface, but cancels with velocity integral terms in the momentum equation integration and does not affect pressure dynamics. Therefore, both the vorticity flux and half-sing vorticity terms can be calculated from the jet velocity program, but the refill impingement vorticity depends on both cavity geometry and jet velocity program.

It should be noted that both the pressure modeling of this section and the impulse modeling of section 4.1.1 were derived and validated for jetting systems in a fixed location. Neither has been validated for thrusters on a moving vehicle.

4.1.3 Modeling Hydrodynamic Inertial and Damping Forces

An alternative approach is to recognize that the total force acting on the UUV, τ_{RB}, is the sum of the control forces, τ_C and the hydrodynamic forces, τ_H, resulting from vehicle motion, $\vec{\tau}_{RB} = \vec{\tau}_C + \vec{\tau}_H$. As such, if the total forces, $\vec{\tau}_{RB}$, and the hydrodynamic forces, $\vec{\tau}_H$, are known then the control forces can be calculated as the difference between the two. The sum of forces acting on the UUV can be determined from the vehicle kinematics and finite rigid body dynamics. The motion capture system described in section 3.2 captures the 6-DOF velocity, $\vec{\nu}$, and acceleration, $\dot{\vec{\nu}}$, of the UUV. The rigid body dynamics described in a frame of reference attached to a rigid body are given using similar notation to Fossen (1994),

$$\vec{\tau}_{RB} = M_{RB}\dot{\vec{\nu}} + C_{RB}(\vec{\nu})\vec{\nu} \ , \tag{7}$$

where M_{RB} and C_{RB} are the mass matrix and centripetal/Coriolis force matrix for the rigid body. When the geometric center of the body lies on the center of mass M_{RB} is the diagonal matrix, diag$\{m, m, m, I_x, I_y, I_z\}$, where I_i is the moment of inertial about the i'th axis and C_{RB} is defined by,

$$C_{RB} = \begin{bmatrix} \emptyset_{3\times3} & C_1 \\ C_1 & C_2 \end{bmatrix} \quad C_1 = m \begin{bmatrix} 0 & w & -v \\ -w & 0 & u \\ v & -u & 0 \end{bmatrix}$$
$$C_2 = \begin{bmatrix} 0 & I_z r & -I_y q \\ -I_z r & 0 & I_x p \\ I_y q & -I_x p & 0 \end{bmatrix}$$

Thus the total forces acting on the vehicle can be calculated from the motion capture kinematic data and the UUV mass and moments of inertia.

The most accurate method for determining hydrodynamic forces would be to measure them directly from a hypothetical pressure/shear sensor networks distributed on the UUV surface Xu & Mohseni (2013), however, that system is still in the process of being developed. In this study we model the hydrodynamic forces with respect to vehicle kinematics, which is fairly standard in the underwater vehicle community. The general equation for hydrodynamic forces on an UUV, as summarized in Fossen (1994) is,

$$\vec{\tau}_H = -M_A\dot{\vec{\nu}} - C_A(\vec{\nu})\vec{\nu} - D(\vec{\nu})\vec{\nu} - g(\vec{\eta}) \ , \tag{8}$$

where, M_A and C_A are the added mass matrix and added centripetal/Coriolis matrix, respectively, D is the drag matrix, and $g(\vec{\eta})$ is a term representing the restorative forces (i.e. buoyancy). As a first order approximation of the various hydrodynamic force coefficients, we treat the UUV as a perfect cylinder with uniform density equal to the surrounding water, and assume symmetry of $C_A(\vec{\nu})$ and $D(\vec{\nu})$ with respect to the radial directions. For such a system,

$$\begin{aligned}
M_A &= \text{diag}\,\{A_{11}, A_{22}, A_{33}, A_{44}, A_{55}, A_{66}\} \\
C_A(\vec{\nu}) &= \begin{bmatrix} \emptyset_{3\times3} & C_3 \\ C_3 & C_4 \end{bmatrix} \\
C_3 &= \begin{bmatrix} 0 & A_{33}w & -A_{22}v \\ -A_{33}w & 0 & A_{11}u \\ A_{22}v & -A_{11}u & 0 \end{bmatrix} \\
C_4 &= \begin{bmatrix} 0 & A_{66}r & -A_{55}q \\ -A_{66}r & 0 & A_{44}p \\ A_{55}q & -A_{44}p & 0 \end{bmatrix} \\
D(\vec{\nu}) &= \text{diag}\,\{D_{11}, D_{22}, D_{33}, D_{44}, D_{55}, D_{66}\} \\
g(\vec{\eta}) &= 0 \ ,
\end{aligned} \tag{9}$$

where A_{ij} are the coefficients of the added mass matrix and D_{ij} are the coefficients of the drag matrix. The principle components of the added mass matrix, A_{ii}, are calculated according to strip theory derived from 2D potential flows Wendel (1956) and UUV geometry. The principle components of the drag matrix are defined as standard high Re drag equations, for $i = [1, 2, 3]$ $D_{ii} = \frac{1}{2}\rho S_i C_{di} |\vec{\nu}|$, $D_{44} = 0$, and for $i = [5, 6]$ $D_{ii} = \frac{\rho L_s^3 d_s}{24} C_{Dy,z} |\nu_i|$. In these expressions S_i are the wetted areas of the UUV in different directions, L_s and d_s are the length and diameter of the UUV, the value for C_{Dx} is taken from Hoerner (1965) for cylinders in axial flow, and the value for C_{Dy} is taken from Hoerner (1965) for cylinders in cross flow. The coefficients approximated for the UUV of this study

are listed below,

$$A_{11} - A_{66} = [2.0\,kg, 20.7\,kg, 20.7\,kg, 0\,kgm, 0.0030\,kgm, 0.0030\,kgm]$$

$$D_{11} - D_{66} = \left[1.87\tfrac{kg}{s}, 14.03\tfrac{kg}{s}, 14.03\tfrac{kg}{s}, 0\tfrac{kgm^2}{s}, 3.63\tfrac{kgm^2}{s}, 3.63\tfrac{kgm^2}{s}\right]$$

In this experiment we operated the UUV near the surface in order to maintain communication using a wireless antenna. Since the UUV is near the surface, the added mass estimates will likely be too high, as added mass coefficients reported for catamarans and bulb sections near the free surface have even become negative for certain frequencies Fossen (1994). In order to improve our estimates of hydrodynamic forces, we calibrate these coefficients using specific portions of the trajectory data when the thrusters are not active. When the UUV has performed a maneuver, and the propulsors are shut off, the vehicle continues to move as the hydrodynamic forces bring it to rest. As an example, figure 5 shows the rotational velocity of the UUV during one of the yaw maneuvers, with the region of inactive drifting marked by the vertical red lines.

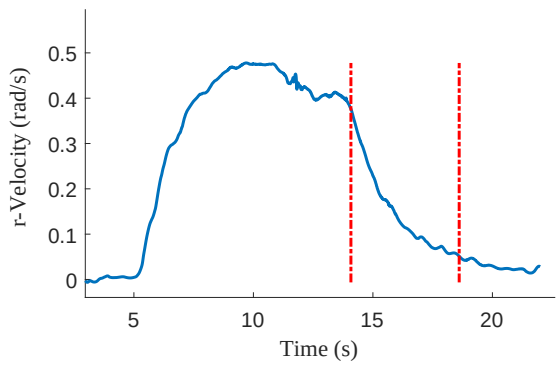

Figure 5: Radial velocity r of the UUV performing an example yaw maneuver. The vertical dashed lines indicate a specific period of this maneuver which is used to calibrate the hydrodynamic force coefficients, since the vehicle is moving through the fluid but there are no control forces acting on it.

During these periods the hydrodynamic force vector, $\vec{\tau_H}$, is identical to the total rigid body force/torque vector, τ_{RB}, calculated from acceleration/velocity data. Thus, unknown hydrodynamic force coefficients can be determined by fitting the motion capture trajectory data for all the maneuver sections without active propulsion. Using an iterative least-squares algorithm, we fit the added mass and drag matrix coefficients, A_{ii} and D_{ii}, to the form (8) with $\tau_H = \tau_{RB}\left(\vec{\nu}, \dot{\vec{\nu}}\right)$, assuming constant coefficients, for all of the trajectory sections with inactive propulsors. The initial guess was set to the analytically predicted coefficients, and coefficients were allowed to vary between zero and 200% of the predicted coefficients. The resulting fitted coefficients near the surface are listed below,

$$A_{11} - A_{66} = [0.52\,kg, 1.97\,kg, 1.97\,kg, 0\,kgm, 0.0029\,kgm, 0.0021\,kgm]$$

$$D_{11} - D_{66} = \left[0.87\tfrac{kg}{s}, 21.05\tfrac{kg}{s}, 21.05\tfrac{kg}{s}, -0.01\tfrac{kgm^2}{s}, 3.54\tfrac{kgm^2}{s}, 3.54\tfrac{kgm^2}{s}\right]$$

The accuracy of the hydrodynamic force modeling is shown in figure 6. In this figure the total rigid body forces/torques, as calculated from vehicle trajectory data, is shown along with the modeled hydrodynamic forces calculated using the coefficients listed above. This figure shows 5 example sections of maneuvering data out of 15 sections used to fit the coefficients.

4.2 Calculating Total Energy Spent on Propulsion

The total work required to create propulsion, just like the useful propulsive work, can be calculated using a number of different techniques. Here we discuss the benefits and shortcomings of 3 different methodologies.

4.2.1 Kinetic Energy in the Wake

The Froude efficiency model, commonly used to discuss propeller efficiency, says that efficiency is inversely proportional to the increase in velocity of fluid passing through the actuator disc plane. Inherent in this concept is a recognition that perfectly efficient propulsion adds kinetic energy to the vehicle, and any kinetic energy added to the wake is wasted. Modern measurement techniques, such as digital particle image velocimetry (DPIV) allow non-intrusive measurement of the wake velocity field. A technique for calculating propulsive efficiency from the wake velocity field is laid out in Krueger (2006), and can be summarized as,

$$\eta_{prop} = \frac{\bar{T}x}{\bar{T}x + E_j}\ , \tag{10}$$

where $\bar{T}$ is the average thrust applied to the body over the motion, x is the distance the body travels, and E_j is the kinetic energy in the wake. Bartol *et al.* used this method to calculate propulsive efficiency of live swimming squid Bartol et al. (2009), challenging notions of the low efficiency of jetting propulsion.

Here we would like to point out that (10) is an accurate representation of efficiency, provided that all wasted energy contributes to the wake kinetic energy, E_j. This is a valid assumption for the majority of underwater locomotory systems; however, there are two energy dissipation mechanisms, that we will discuss in this paper, invalidating such an assumption. One mechanism is viscous dissipation in the wake; and we should note that efficiency calculations in Bartol et al. (2009) corrected for this dissipation, which was determined through personal communication with the

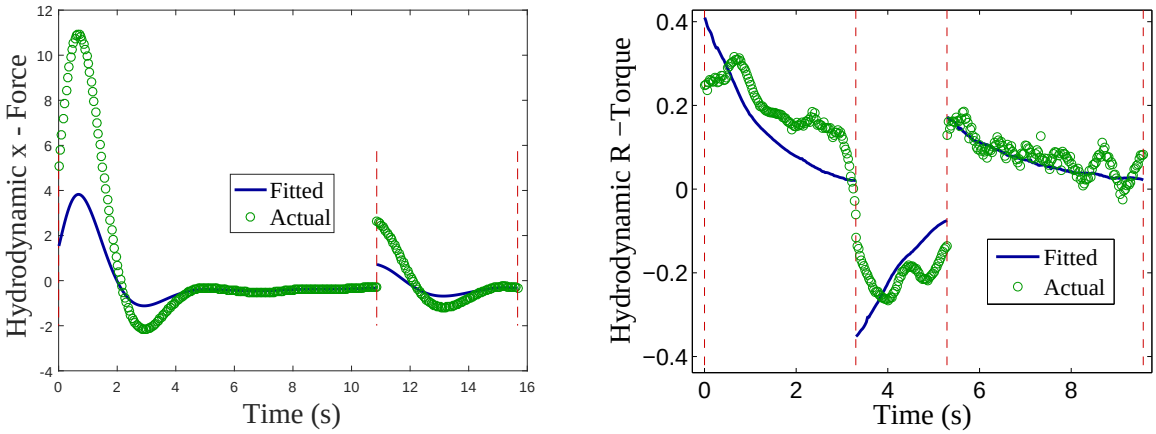

(a) (b)

Figure 6: Accuracy of the hydrodynamic force estimation of the form (8) using constant coefficients fit to data when the propulsors were inactive. Actual hydrodynamic forces acting on the UUV calculated from vehicle accelerations are shown by the circular markers in the body-fixed (a) u and (b) r directions, along with the fitted forces shown by the solid line.

authors. The other mechanism is viscous dissipation inside the jetting cavity (for cases where one exists), and is accelerated by the largely stationary solid boundaries. In general, the degree to which either mechanism affects the efficiency calculation is inversely proportional to the characteristic Reynolds number of the propulsive system.

In the absence of DPIV velocity data of the vehicle wake, models for jet kinetic energy can be used to model the wake for vehicles using jet propulsors. The rate of generation of kinetic energy in unsteady jets under the influence of vortex ring formation is derived in Krieg & Mohseni (2013) as,

$$\frac{dE}{dt} = \frac{\rho\pi}{2}\left(h + \frac{k_2^\star}{2}\right) u_b(t)^3 \frac{R_p^6}{R^4} \,. \tag{11}$$

Here h is a function of the axial velocity profile, and for the nozzle used on the UUV can be set to $h = 1.21$. Integrating over an entire cycle with a sinusoidal jet velocity program gives the jet energy for each pulsation as a function of frequency,

$$E = \frac{16\rho\pi^3 R^5}{3}\left(h + \frac{k_2^\star}{2}\right)\left(\frac{L}{D}\right)^3 f^2 \,. \tag{12}$$

4.2.2 Internal Cavity Pressure modeling

One issue with characterizing efficiency by wake kinetic energy, is that it does not account for energy lost to viscous dissipation in the surrounding fluid. For propulsors like those in this study, where the internal cavity must be refilled in between jetting cycles, the ingested fluid sees significant viscous dissipation inside the bounded cavity before being subsequently ejected. Therefore total work calculations, as described in the previous subsection, will generally give an underestimate of total work spent.

In section 4.1.2 we described modeling for internal cavity pressure that was derived in terms of evolution of system circulation. The pressure distribution calculated by this model can be used to calculate the instantaneous power transferred to the fluid, in addition to the instantaneous thrust. The power required to collapse the cavity boundary is the product of pressure on the cavity surface and the normal component of that surface velocity. For the thrusters of this investigation, the plunger at the back of the cavity is the only part which moves with a velocity normal to its surface. Therefore the instantaneous power for these thrusters is the product of pressure on the plunger P_b, area of the plunger πR_p^2, and the plunger velocity u_b.

4.2.3 Measure Current Draw to the Motor

The simplest way to get the total energy spent on propulsion is to directly measure the current and voltage going from the batteries to the thruster motors. However, the total power going to the motors also includes energy that is lost to friction in the plunger driving system and lost during transmission of electrical to mechanical power in the motor itself. While these losses are important, they are associated with the specific implementation of the propulsion technology and not the intrinsic characteristics of the propulsion technique.

5 RESULTS

In the previous sections we laid out several different methods for calculating both the useful propulsive work, and the total work required for propulsion of a freely moving UUV. In this section we examine the accuracy/agreement of the different techniques.

5.1 Estimating Control Forces

We presented three methods for calculating control forces. These include calculating the hydrodynamic impulse of each jet based on jet velocity program and motor frequency data the dividing by the duration to get average thrust (sec-

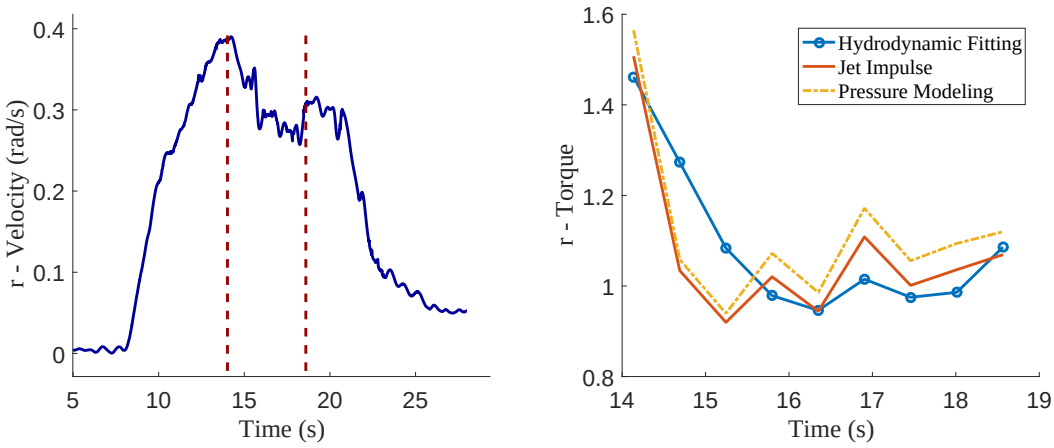

Figure 7: A comparison of control torque about the vehicle fixed z axis during a steady portion of a yaw maneuver is shown on the right. The vehicle rotational velocity during the entire maneuver is shown on the left, with vertical dashed lines showing the period for which the different torque calculation methods are compared.

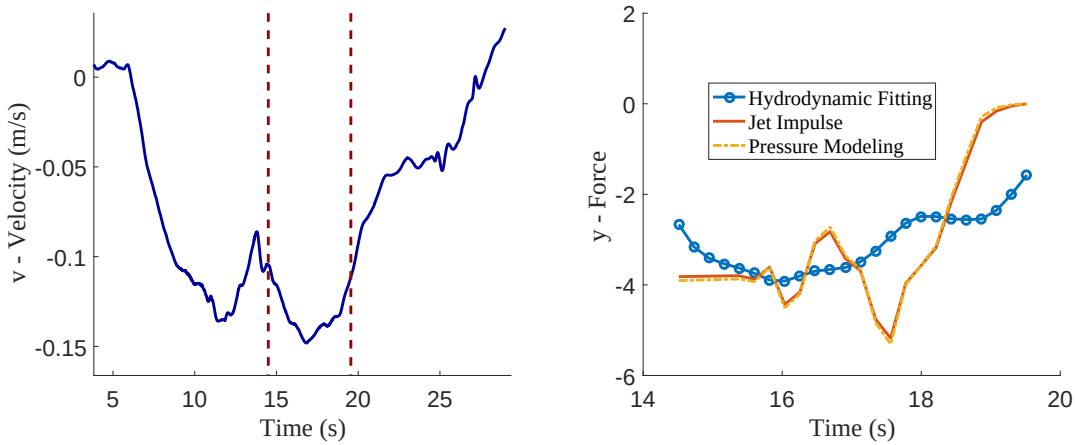

Figure 8: A comparison of control force in the vehicle fixed y axis during a steady portion of a sway maneuver is shown on the right. The vehicle velocity during the entire maneuver is shown on the left, with vertical dashed lines showing the period for which the different force calculation methods are compared.

tion 4.1.1); calculating the instantaneous force from the pressure on the inner surface of the thruster cavity from jet velocity program and motor frequency data (section 4.1.2); and by modeling hydrodynamic forces in terms of vehicle kinematic data, then calculating control forces as the difference between inertial forces and hydrodynamic forces (section 4.1.3). Here we will show that all 3 techniques actually produce similar results for control forces during different maneuvers.

Figure 7 shows the control torque on the vehicle about the z axis during an example yaw maneuver. On the left is the vehicle angular velocity, r, for the entire maneuver. The hydrodynamic forces are calculated with the three different methods after the UUV has reached a more-or-less steady rotational velocity marked by the vertical dashed lines. The torques calculated from the 3 methods over this period are shown on the right. It can be seen that the different methods produce nearly identical estimates of the torque acting on the unrestricted UUV. This not only validates the jet impulse and pressure models for thrusters on moving platforms, but also validates the accuracy of the hydrodynamic force model while the thrusters are active. However, there is significant noise on the motor frequency signal which needs to be corrected in the hardware in order to improve force estimates.

Figure 8 shows the force comparison during a section of a sway maneuver. It can be seen that all 3 models still have good agreement, but the noise on the motor frequency signal is more significant.

The total propulsive work over any given maneuver is the product of these instantaneous control forces and the vehicle velocity, $\vec{\nu}$, (measured by the motion capture system) and integrated over the duration of the maneuver.

5.2 Estimating total Power/Energy

Here we compare the total required work calculations during unrestricted maneuvers. These methods include calculating the kinetic energy of each expelled jet from the motor frequency data and adding that to the the propulsive work done on the vehicle (section 4.2.1), and calculating the instantaneous power transfer to the fluid using the internal pressure model and plunger velocity, then integrating over the pulsation cycle to get total work (section 4.2.2).

Figure 9 shows the total required power output calculated by these two methods during the same yaw maneuver depicted in figure 7. It can be seen that the total power output calculated using the pressure model is nearly 50% greater than the required power calculated from jet kinetic energy. This is mostly due to the fact that there is a non-zero work associated with refilling the thruster cavity in between jetting cycles. This work required to refill the cavity adds kinetic energy to the incoming fluid which is mostly lost to viscous dissipation inside the confined cavity before the fluid is ejected as a propulsive jet. So the total power calculated from the circulation based pressure model should be considered the more accurate method when calculating vehicle propulsive efficiency.

Although the refill work increases the total required work by 50% for this particular velocity program and thruster iteration, it should not be considered a standard proportionality for unsteady jetting propulsion. The work required for refilling is in fact heavily dependent on internal cavity geometry and jetting velocity program. In fact it was shown in Krieg & Mohseni (2015) that energy required to refill the cavity using an impulsive velocity program was nearly half the energy required to fill using a sinusoidal velocity program; and that refill work can be further reduced by inducing impingement earlier on in the refill phase. For a thruster with geometry designed to minimize the refill work, this proportion could be reduced significantly. In the case of the live squid studied in Bartol et al. (2009), there was some non-zero work put into the refilling phase that did not show up in the wake kinetic energy, which would decrease the overall efficiency. However, it is possible, and even quite likely, that squid morphology has evolved to minimize the required refill work, so the decrease in efficiency may not be significant.

CONCLUSIONS

In this study we provided the preliminary work towards experimental testing of the propulsive efficiency of cephalopod inspired jetting technology. We examined three different methods for estimating control forces; modeling propulsive jet impulse, modeling pressure distribution within the thruster mechanism, and backing out control forces from hydrodynamic force estimates and vehicle inertial forces measured with a motion capture system. All three control force measurement techniques showed good agreement for multiple maneuvers, validating the different assumptions of the individual models. We also look into two methods for estimating the power transferred to the surrounding fluid environment required to create the propulsion. It was observed that estimating total required work from the excess kinetic energy in the wake will always under-predict the actual total work due to viscous dissipation of kinetic energy prior to measurement of the wake energy, and that a more accurate estimate can be achieved by integrating the product of pressure and boundary velocity on the surface of the thruster cavity.

Future work includes examining accuracy of the hydrodynamic force modeling during cross-couple maneuvers, examining the accuracy of the jet pressure models when vehicle velocities begin to approach the jet velocity, finding ways to reduce the refill work through cavity geometry, and comparing the overall propulsive efficiency of UUVs employing the cephalopod inspired thrusters to UUVs employing traditional propeller thrusters.

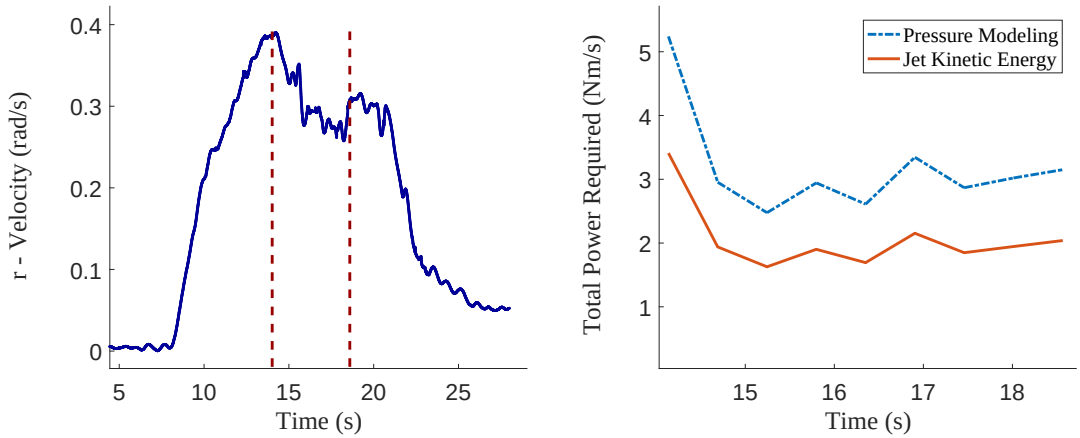

Figure 9: A comparison of total power output spent to generate the propulsion during a steady portion of a yaw maneuver is shown on the right. The vehicle rotational velocity during the entire maneuver is shown on the left, with vertical dashed lines showing the period for which the different energy calculation methods are compared.

ACKNOWLEDGMENTS

This work was sponsored by the Office of Naval Research, Grant #N00014-16-1-2083

REFERENCES

Bartol, I. K., Krueger, P. S., Stewart, W. J. & Thompson, J. T., 2009. 'Hydrodynamics of pulsed jetting in juvenile and adult brief squid Lolliguncula brevis: Evidence of multiple jet 'modes' and their implications for propulsive efficiency'. Journal of Experimental Biology, **212**(12), pp. 1889–1903.

Fossen, T. I., 1994. Guidance and Control of Ocean Vehicles. Wiley-Interscience, Hoboken, NJ, USA.

Hoerner, S. F., 1965. Fluid-Dynamic Drag. Hoerner Fluid Dynamics, Bricktown, NJ, pp. 3–7 – 3–13.

Krieg, M., Klein, P., Hodgkinson, R. & Mohseni, K., 2011. 'A Hybrid class underwater vehicle: Bioinspired propulsion, embedded system, and acoustic communication and localization system'. Marine Technology Society Journal: Special Edition on Biomimetics and Marine Technology, **45**(4), pp. 153–164.

Krieg, M. & Mohseni, K., 2008. 'Thrust characterization of pulsatile vortex ring generators for locomotion of underwater robots'. IEEE Journal of Oceanic Engineering, **33**(2), pp. 123–132.

Krieg, M. & Mohseni, K., 2013. 'Modelling circulation, impulse and kinetic energy of starting jets with non-zero radial velocity'. Journal of Fluid Mechanics, **719**, pp. 488–526.

Krieg, M. & Mohseni, K., 2015. 'Pressure and work analysis of unsteady, deformable, axisymmetric, jet producing cavity bodies'. Journal of Fluid Mechanics, **769**, pp. 337–368.

Krueger, P. S., 2005. 'An over-pressure correction to the slug model for vortex ring circulation'. Journal of Fluid Mechanics, **545**, pp. 427–443.

Krueger, P. S., 2006. 'Measurement of propulsive power and evaluation of propulsive performance from the wake of a self-propelled vehicle'. Bioinspiration and Biomimetics, **1**(4), pp. 49–56.

Lighthill, M. J., 1969. 'Hydrodynamics of aquatic animal locomotion'. Annual Review of Fluid Mechanics, **1**, pp. 413–445.

Mclean, M. B., 1991. Dynamic performance of small diameter tunnel thrusters. Ph.D. thesis, Naval Postgraduate School, Monterey, California.

Mohseni, K., 2006. 'Pulsatile vortex generators for low-speed maneuvering of small underwater vehicles'. Ocean Engineering, **33**(16), pp. 2209–2223.

Vogel, S., 1994. Life in Moving Fluids. 2nd ed. Princeton University Press, Princeton, NJ.

Wendel, K., 1956. 'Hydrodynamic Masses and Hydrodynamic Moments of Inertial'. Tech. Rep. Jahrb. d. STG, Volume 44", Navy Department.

Xu, Y. & Mohseni, K., 2013. 'Bio-inspired hydrodynamic force feed forward for autonomous underwater vehicle control'. IEEE/ASME Transactions on Mechatronics, **19**(4), pp. 1127–1137.

Yoerger, D., Cooke, J. & Slotine, J.-J., 1990. 'The influence of thruster dynamics on underwater vehicle behavior and their incorporation into control system design'. IEEE Journal of Oceanic Engineering, **15**(3), pp. 167–178.

DISCUSSION

Question from Tom Van Terwisga Could you explain to me how you separate the hydrodynamic forces on the AUV from the control forces in method of 'extraction of the force from motion dynamics'?

Author's Response Here we apply a standard model for the hydrodynamic forces assuming that they are a function of the vehicle kinematics as described in section 4.1.3. The various coefficients (stability derivatives) that relate the different components of hydrodynamic forces to various components of vehicle velocity and acceleration are calibrated from AUV trajectory data during periods when all thrusters have been turned off, hence zero control forces. Once this model has been calibrated, it is used to calculate hydrodynamic forces over the entire testing period, and control forces are calculated as the difference between the total rigid body forces and the modeled hydrodynamic forces. This is then validated by comparing with the other methods for estimating control forces.

Follow up Question Do I correctly understand that you assume that the thrust influence of the jet-hull interaction is equal to zero? Do you know what sort of error is involved in that assumption?

Author's Response Yes we are assuming that the drag coefficients of the vehicle are unaffected by the jet flow when the thruster is turned on. If we examine the 2D flow over cross sections of the vehicle at the thruster opening location the jet flow will eliminate the rear stagnation point, which will certainly have an effect on the drag profile of that section. Since these thrusters are being used for maneuvering, the jet flow will only affect the flow over a small portion of the length, and thus the effect on hydrodynamic forces will be negligible. However, if the thrusters are being used for forward propulsion, the jet flow will have a significant effect on the vehicle drag and the method for extracting control forces by subtracting off hydrodynamic forces will not be as effective.